Published in Journal of the Electrochemical Society 162(10) E213-222, July 2015.

The effect of initial etching sites on the morphology of TiO_2 nanotubes on Ti-6Al-4V alloy

U. Danookdharree[1], H. R. Le[1] and C. Tredwin[2]

[1]School of Marine Science and Engineering, Plymouth University, Plymouth, United Kingdom.

[2]Peninsula Schools of Medicine and Dentistry, Plymouth University, Plymouth, United Kingdom.

Address correspondence first to HL: huirong.le@plymouth.ac.uk, second to UD:

urvashi.danookdharree@plymouth.ac.uk

Abstract

Anodisation was performed in phosphate and fluoride containing electrolytes at different pH and sweep rates with the aim of analysing the variation in current density during the process continuously. The effect of pH and sweep rate on the morphology of titanium dioxide (TiO_2) nanotubes, grown on Ti-6Al-4V alloy, has been explicitly examined in this study. At the same time a microscopic analysis of the different stages of the formation of the nanotubes was performed. A new perspective to the growth mechanisms of the nanotubes was brought about in this study. The morphology of the nanotubes was closely related to the density of initial etching sites.

Keywords: Titanium dioxide, nanotubes, Ti-6Al-4V, anodisation, morphology, sweep rate, pH

1. Introduction

Surface modification of bone and dental implants at micro and nano-level has attracted significant interest in the last decade. The application of such modification to titanium and its alloys has a positive effect on the bioactivity property of the latter [1]–[3]. This effect has been partly ascribed to the biomimicking of bone nanostructure [4]–[7]. Meanwhile, the nano-modification acts as a coating preventing the leaching of ions, such as vanadium and aluminium in the case of Ti-6Al-4V, from the implant's surface, as such, preventing the loosening of the latter and avoiding further complications[8]–[10]. Converting the nanostructured coating to a porous tubular structure, can make the latter act as a drug carrier [11], [12]. Antibacterial agent is one example of the drugs that can be inserted to add antibacterial properties to the surface.

Several methods have been employed for the self-assembly of nanotubes on titanium surface, out of which anodisation is a successful electrochemical process having the ability of producing well defined nanotubes. The procedure involves different types of electrolytes, among which aqueous electrolytes have been shown to allow the manipulation of the morphology of the nanotubes while generating rough exterior walls as compared to non-aqueous ones. Such property has been associated with stronger adhesion forces between the nanotubes [13][14]15]. Since one of the objectives of this work was to produce good adhesion for the nanotubes coating, aqueous electrolytes were used.

Apart from the presence of water, the ions in the electrolytes also have a role to play in the fabrication of the nanotubes. They are involved in both the oxidation and etching processes during the electrochemical process. In this study phosphate ions were used because of their pH buffering capacity in association of fluoride ions which are responsible for the etching process mainly [16]–

[18].

There are additional parameters affecting the self-assembly of the nanotubes on titanium or its alloy such as the pH of the electrolyte, voltage, temperature and duration of anodisation. The pH of electrolyte and the duration of the anodisation have been shown to affect the thickness of the coating. In 2005, Cai and colleagues, published their work whereby they observed the increase in height of nanotubes, formed in the presence of sulphate ions. For the growth duration of 20 hours, at 10V, the thickness of the nanotubes increased from 0.32 μm to 1.40 μm when the pH was changed from 1.3 to 5.0 [19]. Paulose and associates worked with sulphate ions similarly for just 30 minutes and observed the same pattern with nanotubes length being 0.35 μm at pH 1.1 and 2 μm at pH 5.0 [20]. Even when phosphate ions were used by Matykina and co-workers, the same pattern was observed with a height of 0.32 μm at pH 4.2 and 1.75 μm at pH 4.6 [21]. Moreover, increasing the duration of the anodisation process increases the thickness too [8], [22], [23]. At the same time, the anodisation voltage has been shown to affect both the diameter and length of the nanotubes. The group of Schmuki demonstrated the change of diameter from 15 to 120 nm and length from 20nm to 1μm with respect to voltage variation from 1 to 25V [24]. However several studies focusing on the effects of the applied voltage showed that there is a limit in the increase in diameter. Those papers emphasized on the effects of voltage applied in the anodisation process. Nonetheless little attention was given to the effect of the initial voltage ramp in phosphate containing electrolytes on the nanotubes morphology. Taveira and colleagues did examine the effect of the initial ramp and their results indicated that the initial formation of the barrier layer, which was considered to have a major role in the final morphology obtained was dependent on the sweep rate [23][25]. Consecutively, it could be presumed

that the initial change in voltage affects the interfacial adhesion between the nanotubes and the substrate. These authors however concentrated their work on the morphology of the nanotubes grown in sulphate containing electrolytes and did not consider the adhesive strength of the coating.

Following the initiation stage, the nanotubes are self-assembled by the competition between the oxidation and chemical dissolution. The process as to why the nanotubes are uniformly arranged had been described by different groups [26][27]. The group of Dikova performed a step by step analysis of the nanotube formation in hydrofluoric acid at 25 V and provided microscopic images of the different structures at different intervals. Meanwhile, the group of Macak used ammonium sulphate in the presence of fluoride ions at 20V in order to obtain nanotubes with an average diameter of 100nm. They concentrated on the changes in morphology during the formation of the nanotubes especially with the change in pH but they did not analyse the different stages of formation.

This is what motivated this study to aim at analysing the effect of pH and sweep rate on the final morphology of the nanotubes formed on medical grade titanium alloys in phosphate and fluoride containing electrolytes. This research work also looked into the different stages of nanotube formation in order to understand how the respective morphology was developed.

2. Experimental

2.1 Materials

Medical grade 5 Ti-6Al-4V titanium alloy having 6% aluminium and 4% vanadium was laser-cut into discs of 15mm diameter and 1 mm thickness. The polishing with sand paper (#600-1200) was done using a rotary instrument (Grinder-Polisher, Buehler, UK Ltd, Coventry, UK). The cleaning (Sodium carbonate, Na_2CO_3; Sodium Hydroxide, NaOH and Sodium Citrate, $NaH_2C_6H_5O_7$) and anodisation

(Ammonium Sulphate, $(NH_4)_2SO_4$; Ammonium dihydrogen Phosphate, $NH_4H_2PO_4$; Ammonium Fluoride, NH_4F) stages were performed using solutions prepared from reagent grade chemicals from Sigma Aldrich (UK). The power for the anodisation process was supplied from a programmable power supply and the pH and temperature were measured using a Seven Compact™ pH/Ion Meter S220, both purchased from Metrix Electronics Limited. Roughness measurements were done using a LEXT OLS 3000 confocal laser microscope. Microscopic images were obtained using a field emission scanning electron microscope (FE-SEM JEOL 7001F) which was combined with an Oxford Instrument AzTEC energy-dispersive x-ray spectroscopy (EDS) in the Electron Microscopy Centre at the University of Plymouth.

2.2 Self-assembly of nanotubes

The discs were polished using #500-1200 silicon carbide paper followed by a diamond paste finishing to R_a roughness of less than 100 nm from R_a roughness more than 300 nm. Anodisation was then performed using 0.2- 0.5 wt% (weight percent) ammonium fluoride and 0.5-1 M (mole/litre) ammonium dihydrogen phosphate after an alkaline cleaning in an ultrasonic bath. The sweep rate was varied from 0.2-1.5 Volts per second (V/s) from zero to 20V using a personalised Labview program. The latter would communicate with the power supply which in turn ramped the voltage supplied to the anode and

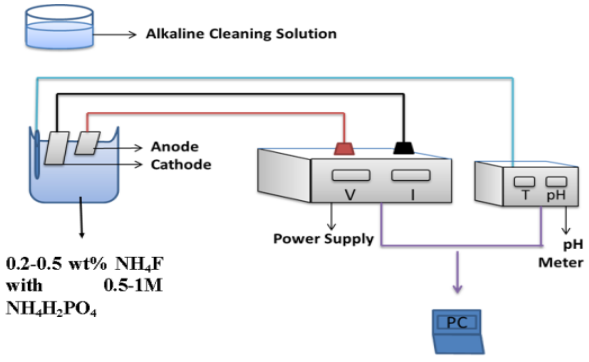

Figure 1: Anodisation process followed by adhesion test

cathode in the electrolytes. The set-up was as shown in Figure 1. The pH was adjusted using aqueous sodium hydroxide (3M), for more alkalinity and aqueous phosphoric acid (3M) for more acidity. The pH range used was from 3 to 6. The current value was recorded at every 0.2s for 3600 s.

2.3 Analysis of nanotubes

The nanotubes formed were initially, qualitatively, analysed using SEM associated with the EDS analysis. From the results, the average diameter, wall thickness and composition of elements present in the coating were then acquired at different formation stages. Furthermore, the porosity of the coating was calculated using Matlab image analysis. The steps taken were as follows:

1) Initial cropping of the image, in order to remove the labels.
2) Contrast enhancement aiming at adjusting the pixel intensity.
3) Application of median and average filter in order to smoothen the image.
4) Otsu's Method of thredsholding was performed to distinguish in between intensities.
5) The image was then converted to black and white
6) The porosity was then calculated using the following formula:

$$\text{Porosity} = \frac{Number\ of\ Black\ pixels}{Total\ Number\ of\ pixels}$$

3. Results and Discussion

The current value recorded during the whole anodisation process was analysed and correlated with the SEM images of the sample. This resulted in the understanding of the different stages of nanotube formation.

3.1 Anodising current variation

The anodising current densities varied with respect to time, as shown Figure 2, during the process of nanotube fabrication. The time and current density values are approximate values at an initial sweep rate of $0.5Vs^{-1}$. The values were used to compare the difference at various stages of the experiment.

It could be observed that in the first second, there was a steep increase in current density to a very high value, in the range of 10 mA mm^{-2} (Peak A), as compared to the whole process. It decreased within the first second itself. The rise to peak A happened in order to develop an electrode potential at the anode as soon as a circuit was made. There was a fast rate of electron transfer between the electrolyte and the electrode during that second. This current was determined by the initial resistance of the electrolyte. Subsequently the current density increased to a maximum of $0.5mAmm^{-2}$ (B) when the voltage was about 10 V (that is half way during the change in the anodising voltage). It then decreased to a minimum point after which it increased slightly during part C until 20V was reached, The current density stayed momentarily at that value to follow a minor decrease after which it stayed almost constant for one hour. This was associated with the fact that the equilibrium of the electrochemical cell was reached.

Between the decrease from peak A to the increase to peak B, there was no detectable current for about 500 ms, (From 1 to 1.5 s) as shown in Figure 3 (a). This was associated with the ideal polarisable electrode (IPE) as even though there was a change in voltage, no charge was flowing between the electrolyte and electrode. Therefore the electrical double layer at the solution/electrode interface acted as a capacitor. When the electrode potential was applied, some of the ions from the electrolyte got adsorbed on the surface of the electrode giving rise to desolvated ions [28]. Hence the double layer was formed by firstly, the solvent molecules along with the adsorbed ions and secondly

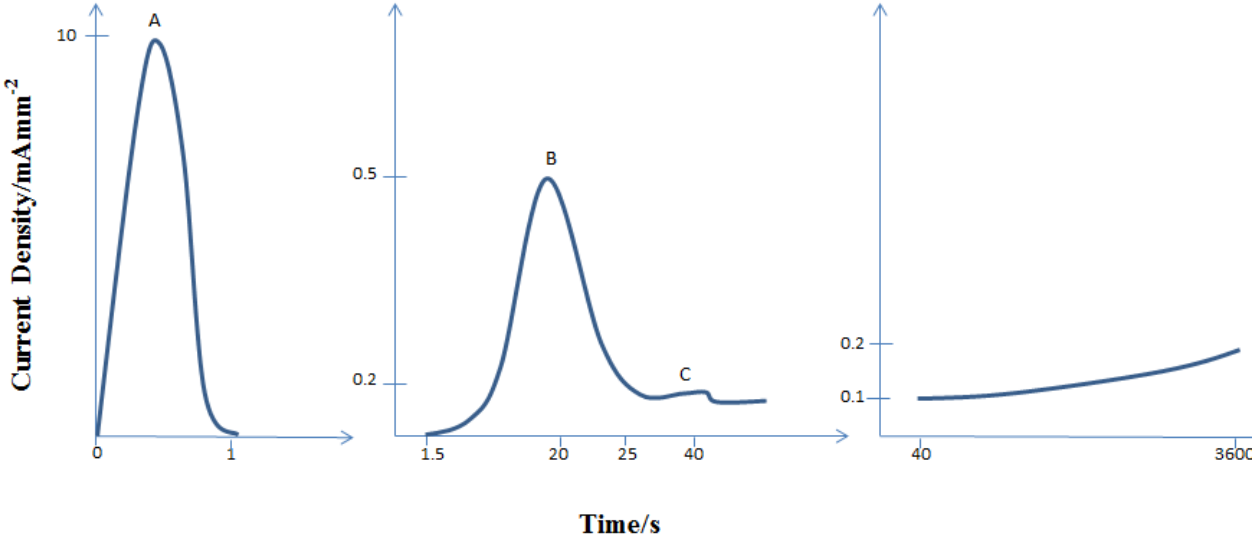

Figure 2: Current Density variation during anodisation

the solvated ions in the electrolyte as shown in Figure 3(b). In this situation the capacitance was dependent on the potential applied and the effect was independent of the content of the electrolyte.

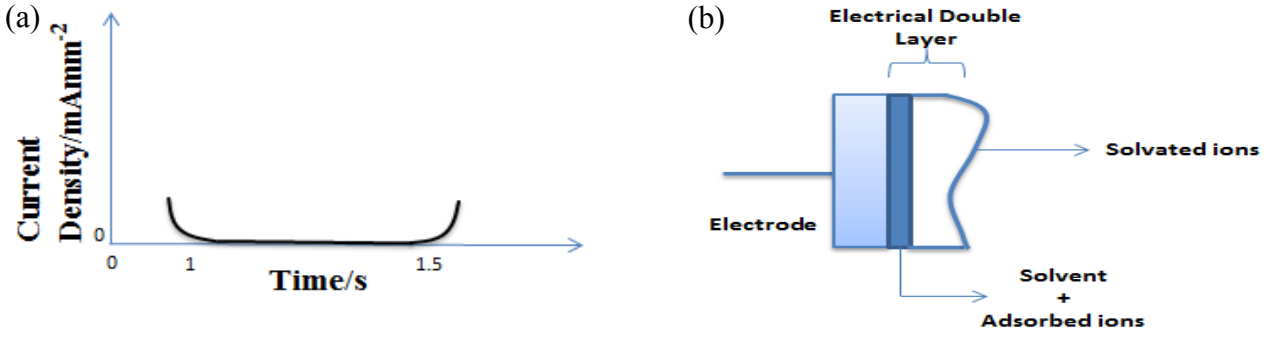

Figure 3: (a) Current density variation during the anodisation whereby the IPE effect was seen and (b) the presence of the electrical double layer

The increase to peak B occurred due to the resistance of the electrolyte and was considered to be non-Faradaic and was related to Ohm's law. Therefore according to Ohm's equation, $V=IR_s$ (R_s is the resistance of the solution), the current density increased, as the voltage increased, to peak B. It

stopped increasing at that point as the potential for barrier formation was reached.

The following decrease was due to the formation of the barrier layer on the titanium alloy sample ($Ti^{4+} + 2\ O^{2-} \rightarrow TiO_2$....(i)). This decrease in current can be explained using the following equations:

$i = \alpha \exp(\beta E)$.....(1);

$i = \alpha \exp(\beta U/d)$.....(2);

whereby i is the current density, E is the electric field across the oxide layer and U is the voltage across the oxide with thickness, d (1). According to equations (1) and (2), as the thickness of the oxide layer d is increased, the current density would decrease exponentially.

The current density increased slightly until peak C where the voltage reaches the level of 20V. This increase is owing to the increase in voltage and the polarization of the anode. The current density drops after the voltage reaches the maximum 20V and the polarization stops. The gradual increase in the current density after peak C was due to the etching of the oxide layer in the presence of the F^- ions which react with the TiO_2 layer forming soluble $[TiF_6]^{2-}$ ions ($6F^- + TiO_2 + 4H^+ \rightarrow [TiF_6]^{2-} + 2H_2O$…..(ii)). This reaction becomes almost constant when equilibrium between oxide layer formation and etching was reached. Therefore there was a further equilibrium (ii). As such the rate of oxide formation equated the rate of chemical dissolution. Following the theory mentioned by Macak and colleagues, the dissolution allowed the nanotubes to grow deeper in the oxide layer while the continuous oxidation helped the nanotubes to grow longer (2). In the meantime small nanotubes will disappear leaving the larger nanotubes leading to a small increase in nanotube diameter and porosity with time. Therefore a small increase in current density is observed.

The different parts of the anodisation curve (peak A and B and part C) would be used as a reference in

the following subsections in order to be able to analyse the different parameters with respect to those part of the anodisation curve.

3.2 Effect of pH

While the pH value was varied, the initial sweep rate was maintained at $0.5Vs^{-1}$. The change was found to affect the anodising current variation with respect to time and voltage, especially in the initial stage which is crucial in the formation of the nanotubes.

In Figure 4, no pattern was visible in the increase in current density to peak B. This was because this part was independent of the reactions. It was mainly dependent on the resistance of the electrolytes which was reliant on the rate of electron transfer.

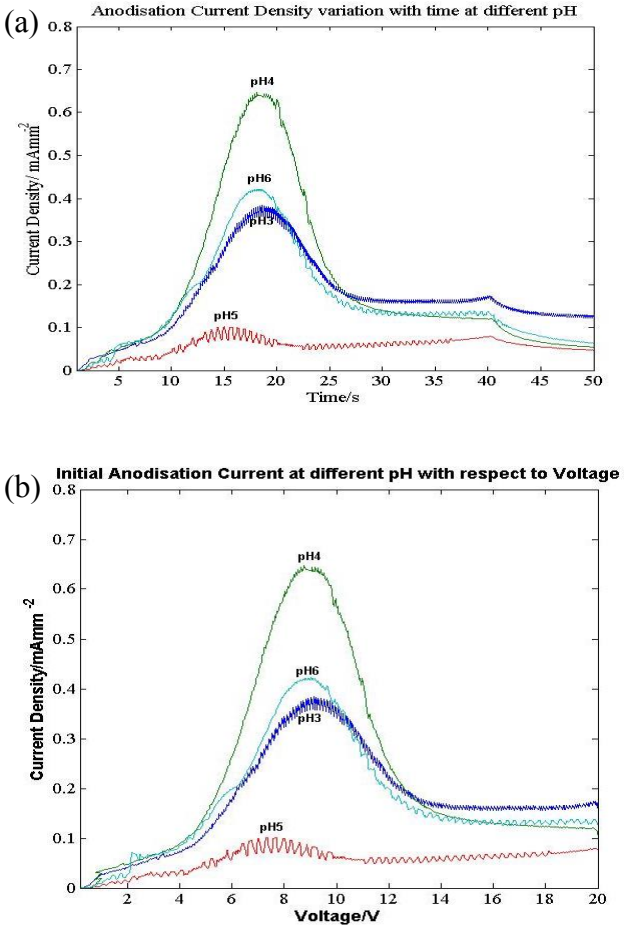

Figure 4: Anodisation Current Density variation at different pH with (a) time and (b) voltage at SR 0.5V/s

No visible pattern again was observed in the formation of the barrier oxide layer both in the peak value and the rate of change in current density. However the etching was dependent on the pH. The final value reached just before equilibrium was higher at a lower pH even though faster etching was expected in the

presence of more hydrogen ions. This can be explained by the etching and oxidation process on the oxide-metal interface. The etching reaction (ii) is the slowest process among them, as such could be chosen as the rate determining step. The etching process was a temperature dependent reaction (Arrhenius type relationship) and followed Fick's Law of diffusion. Therefore it was characterised by the following equation:

$$i = \alpha \exp\left(\frac{-\Delta G}{RT}\right) \quad \text{(3);}$$

whereby α is a constant, R is the gas constant, T is the temperature and ΔG is the Gibbs energy change.

At chemical equilibrium,

$$\Delta G = \Delta G^{o} + RT \ln Q \quad \text{(4);}$$

Whereby G^{o} is the maximum amount of energy change happening and Q is the reaction quotient dependent on the reactants in the reaction and can be expressed as follows:

$$Q = \frac{[TiF6^{2-}]}{[H^{+}]^{4}[F^{-}]^{6}} \quad \text{(5);}$$

Thus at equilibrium,

$$i = \frac{\alpha}{Q} \exp\left(\frac{-\Delta G^{\circ}}{RT}\right) \quad \text{(6);}$$

$$i = \alpha \frac{[H^{+}]^{4}[F^{-}]^{6}}{[TiF6^{2-}]} \exp\left(\frac{-\Delta G^{\circ}}{RT}\right) \quad \text{(7);}$$

Since the energy change to the electric field by the following:

$$G^{o} = -nFE^{\circ} \quad \text{(8);}$$

the current density can be related to the concentrations of different ions as follows:

$$i = \alpha \frac{[H^{+}]^{4}[F^{-}]^{6}}{[TiF6^{2-}]} \exp\left(\frac{nFE^{\circ}}{RT}\right) \quad \text{(9);}$$

These equations were correlated with the etching process whereby the current density was dependent

on the reactants, the number of electrons involved and the field potential. The concentration of fluoride ions was determined by the concentration of NH_4F while the concentration of H^+ was determined by pH. The lower the pH, the higher the H^+ concentration, as suchleading to higher current density.

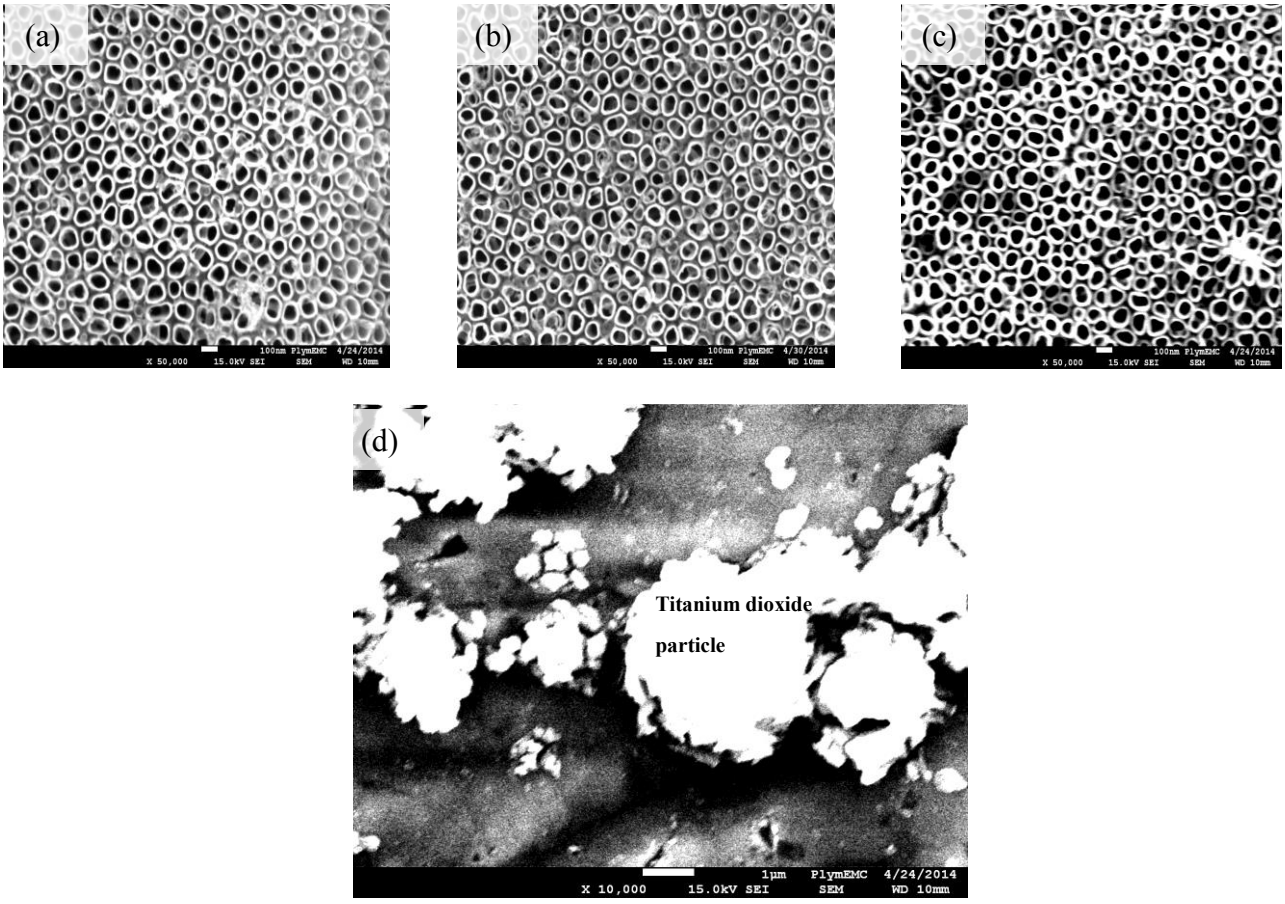

Figure 5: Surface microscopic view of nanotubes coating grown at 0.5 Vs^{-1} and (a) pH 3, (b) pH 4, (c) pH 5 at 50 000 magnification and (d) pH 6 at 10 000 magnification

However, pH 6 was an exception. This could be associated with the fact that when doing anodisation at pH 6, hydroxide particles were formed along with the formation of nanotubes. This could be further explained by the associated high resolution microscopic images. Figure 5 showed the different

microscopic image of the coating formed after anodisation for 3600 s. It could be observed that from pH 3 to pH 5, nanotubes were formed with a uniform distribution with the number of nanotubes being higher at pH 5 than at pH 3 with thicker walls. This observation would be further discussed below. The observation at pH 6 could be explained by the fact that the concentration of H^+ ions was lower and could be better explained by the following equations:

$[TiF_6]^{2-} + nH_2O \rightarrow [TiF_{6-n}(OH)_n]^{2-} + nH^+ + nF^-$ ……..……..(iii)

$[TiF_{6-n}(OH)_n]^{2-} + (6-n)\ H_2O \rightarrow [Ti(OH)_6]^{2-} + (6-n)\ H^+ + \ (6-n)\ F^-$ ……(iv)

$[Ti(OH)_6]^{2-} + 2\ H^+ \rightarrow TiO_2 + 4H_2O$ ……..…….....(v)

Normally following the above reactions, titanium dioxide nanotubes were expected to form. However at pH 6, the presence of lower concentration of H^+ ions causes a reduction in reaction (v), allowing the accumulation of titanium hydroxide which later decomposed to oxide particles.

Figure6 (b) showed how the final current density value decreased from pH 3 to pH 4 and slightly higher at pH 5 than that at pH 4The diameter of the nanotubes was found to be affected by about 10 nm for every increment in pH. The final current value at pH 5 and pH 6 was found to be higher due to the additional particles being formed on the surface of the alloy. It was noted that even though the wall thickness increased with increasing pH, the general diameter of the nanotubes was found to be decreasing. Figure 6 (b) also showed that there was an increase in porosity with increasing pH while Figure 7 highlighted the higher current density change during the last 30 minutes of anodisation at pH 6. The current density values at pH 3, 4 and 5 were lower than that at pH 6 further highlighting the effect of increase in hydroxide concentration. Nanotubes formed on titanium or its alloy can have a U-

shape or a V-shape [11], [29][30]. Chen and colleagues further demonstrated the effect of temperature on the resulting shape. Gradual increase in temperature led to the formation of a U-shape and steady temperature led to the growth of V-shaped nanotubes. Since the anodisation in this work was done at steady room temperature, V-shaped nanotubes were expected. Figure 8 emphasized on the change in pore diameter in with height of nanotube as per previous researches. This effect has been seen in nanotubes formed in the presence of phosphate ions as well [31]. During the review of the literature, there was an emphasis on the effect of pH on the thickness of titania nanotubes whereby longer nanotubes were obtained in electrolytes having a higher pH. Combining both theories related to the growth of titania nanotubes, the longer nanotubes formed at a higher pH would be expected to have a larger pore diameter as compared to the short nanotubes formed at lower pH. However in this study it was found that the pore diameter becomes smaller with increasing pH. This was associated with the fact that at a higher pH, the hydrogen ions mediated reaction (equation (ii)) was reduced. Therefore

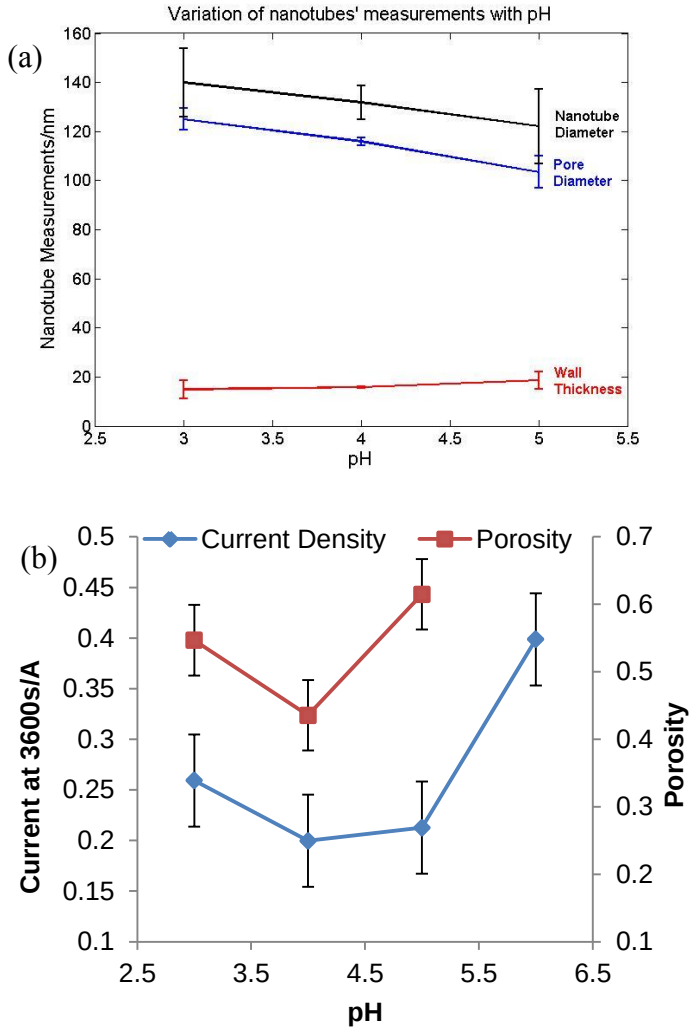

Figure 6: (a) Nanotube morphology and (b) Final Current value variation with pH

the wall thickness did not decrease with increase in the length of the nanotubes. Meanwhile more nanotubes were grown at pH 5 (144 nanotubes per square micrometer) as compared to pH 3 (72 per square micrometer). The number of nanotubes was doubled in quantity when pH increased from 3 to 5. This could be explained by the fact that the etching started earlier at a lower pH. This resulted in larger etching sites at a lower pH and hence accounting for fewer sites on a specific area as shown in Figure 5. At a higher pH, the rate of oxidation was quicker as such more nanotubes were formed per unit area and hence smaller in diameter, as illustrated by Figure 5.

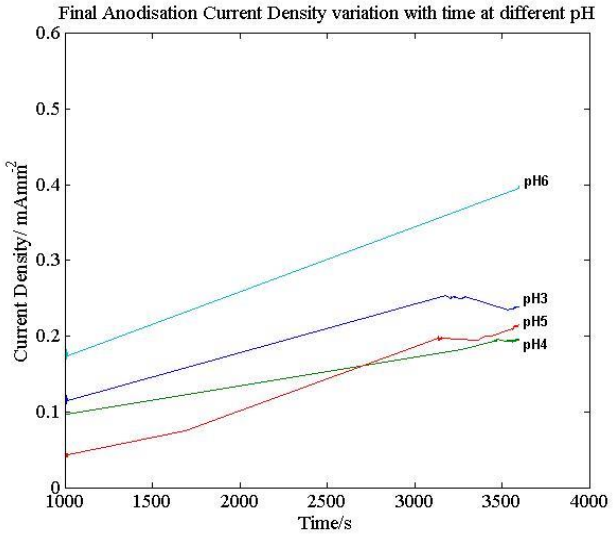

Figure 7: Variation of current density with time for the last 30 minutes at different pH

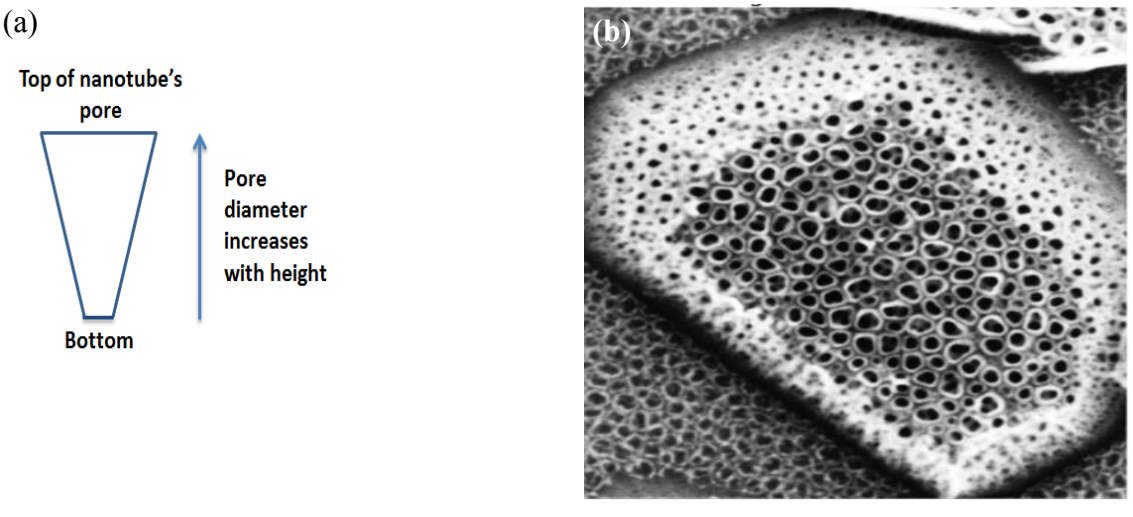

Figure 8: (a) V-shape nanotube depicting change in pore diameter (b) Cross section of nanotubes at different heights showing smaller pores at the bottom and larger pore at the top.

3.3 Effects of Sweep Rate

The value and the rate of change in current density increased with increasing sweep rate prior to the peak B in Figure 9. The general increase was because for the same time period a larger voltage was applied to the system. As such following Ohm's Law, the current value would be higher at a specific time at a higher sweep rate. Although the final potentials reached by all the systems were the same, it could be observed that the maximum current density value reached was higher with increasing sweep rate, as shown in Figure 9. The general increase could be correlated with a larger power density being applied at SR1.5 in order to form the oxide barrier layer as compared to SR0.2. As such a greater stress would be generated at the electrode/oxide interface at a higher sweep rate. It was also observed that the reaction at sweep rate 0.8 Vs^{-1} does not follow the pattern. In fact the maximum current density reached did not change massively at sweep rate between 0.5 Vs^{-1} and 1.0 Vs^{-1}. It could be presumed that the barrier layer was

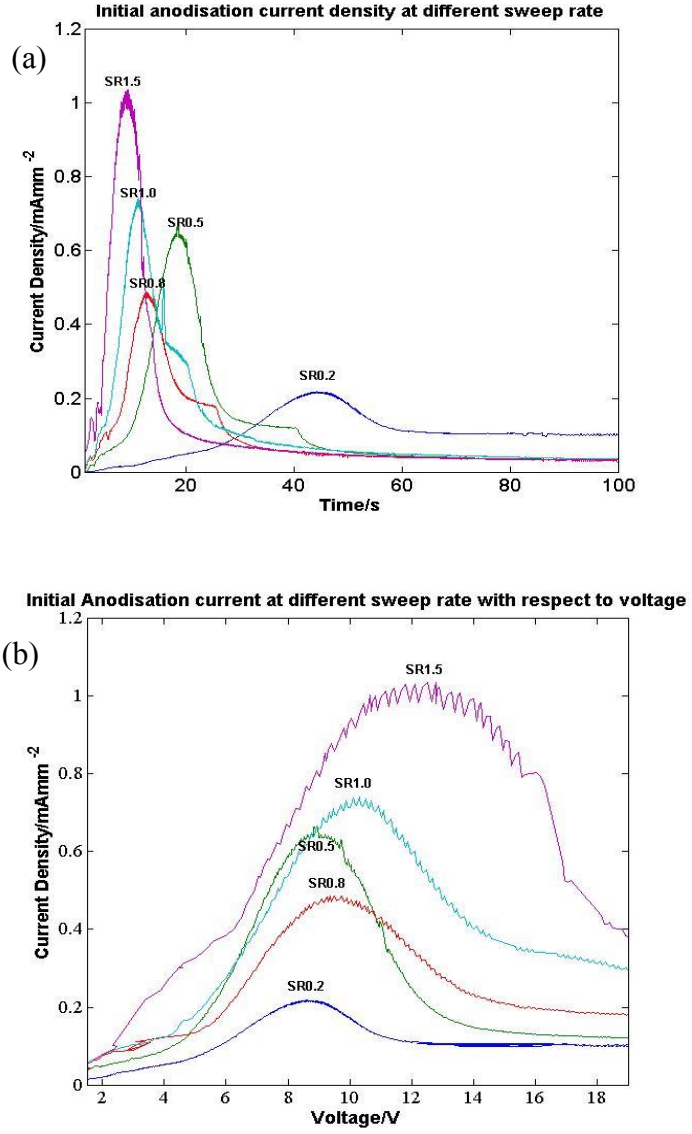

Figure 9: Current density variation with respect to (a) time and (b) voltage at different sweep rate

formed with the appropriate stress needed when the anodisation was done between those two sweep rates. A faster sweep rate (e.g. 1.5 Vs^{-1}) would cause higher stress and more defects in the barrier layer and hence higher maximum current density. On the other hand a very slow sweep rate (e.g. 0.2 Vs^{-1}) would generate less stress for the barrier formation.

Figure 9 (b) highlighted the start of etching at a lower voltage at SR0.2 as compared to SR1.5. Basically because of a longer time taken to reach 20V at SR 0.2, part C of the anodisation curve was supposed to occur later as compared to SR 1.5. This was visible in Figure 9 (a). However peak C was reached at a higher voltage at SR1.5 than at SR 0.2. And at the highest sweep rate peak C was not even reached prior to 10V. This would mean that at a lower sweep rate a smaller potential was required before etching could occur. A justification for this behavior would be that at SR0.2, lower impedance was encountered so that the total voltage is lower when etching occurs. This could be confirmed by the area under the graph in Figure 9 (b) whereby at SR 1.5, larger impedance was encountered during etching.

Figure 11 showed a general decrease in the pore diameter of the nanotubes with increase in sweep rate. The value decreased from about 120 nm at sweep rate 0.2V/s to about half that value at sweep rate 1.5V/s. It was also observed that the wall thickness of the nanotubes slightly increased as visible on the microscopic images in Figure 10. The final current density value followed the same pattern as pore diameter shown in Figure 11(b). The porosity however remained unchanged. This was because as the sweep rate increased the number of etching sites increased as well. However since there was a decrease in the diameter of the nanotubes, these two parameters counteracted each other causing the porosity to stay almost the same at the different SR.

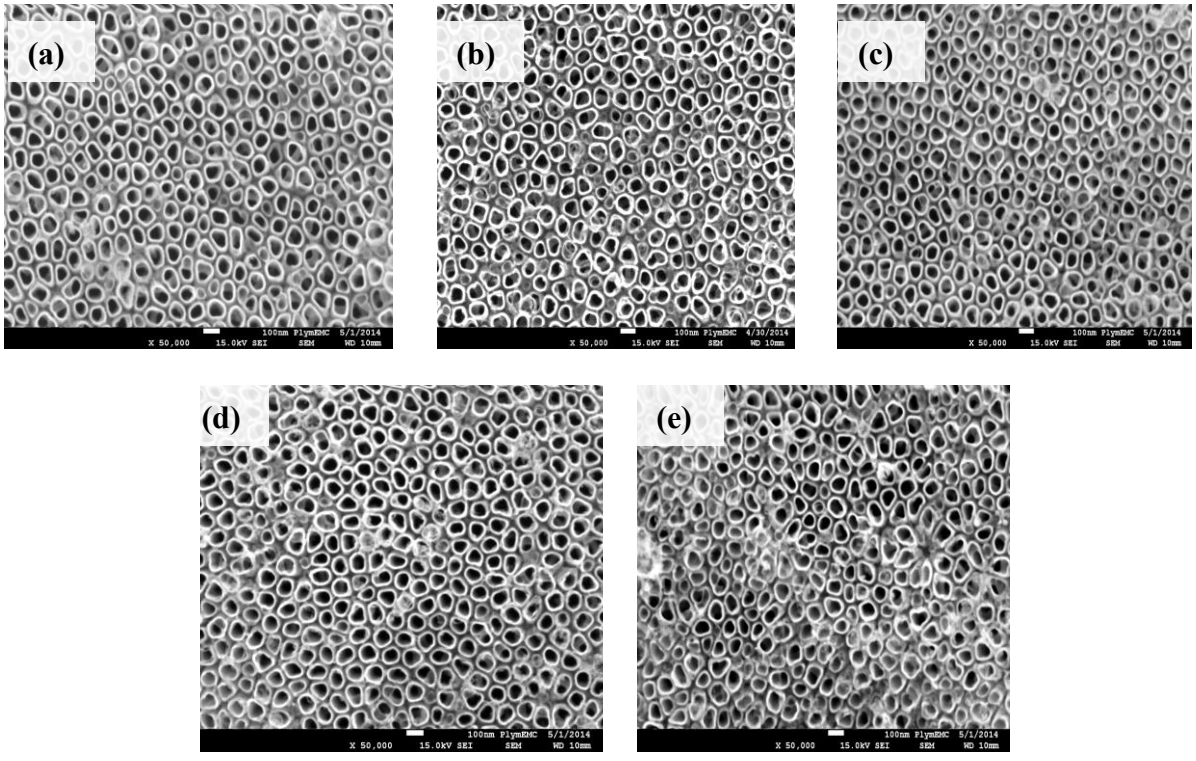

Figure 10: Microscopic images of the TiO2 nanotubes coating at pH 4 and sweep rate (a) 0.2, (b) 0.5, (c) 0.8 (d) 1.0 and (d) 1.5 Vs^{-1}

This would lead to the conclusion that there were more etching sites at a higher sweep rate so that more nanotubes were formed per unit area as shown in Figure 10. Figure 12 zoomed in on the change in current density for the last 30 minutes of the process and it was seen that the current values were lower at higher sweep rates in general even though the maximum current reached at the beginning was higher. This could be correlated with the pore diameter shown in Figure 11. The lower the pore diameter, the lower the current density due to increased resistance to ion diffusion.

3.5 Stages of nanotube formation

The different stages of the fabrication of nanotubes were analyzed by stopping the anodisation at different time and then analysing the resulting substrate using the SEM. The detailed images were

presented in Figure 13. After the formation of the barrier layer, etching was seen to take place before 20V was reached, due to the presence of nanoparticles of average diameter 25nm, not well-defined. Five minutes after 20V was reached, it was observed that the beta phase was more etched than the alpha phase. At the same time, small doughnut-shaped pores were formed with diameter ranging from 50nm to 100nm.

Following Figure 13, it was observed that with time, more etching was taking place with increased size of the nanoparticles to about 100 nm. At 10 minutes (Figure 13 (b)) the beta phase was further etched with the presence of nanograins (100 nm). Five minutes after this, the nanoparticles were further etched giving rise to nanoporous structures with pores (50nm -100 nm) in the beta phase as shown in Figure 13 (c). The dissolved nanoparticles were believed to be vanadium oxide. This was because vanadium oxide is highly soluble. Vanadium is the β-stabiliser in a Ti-6Al-

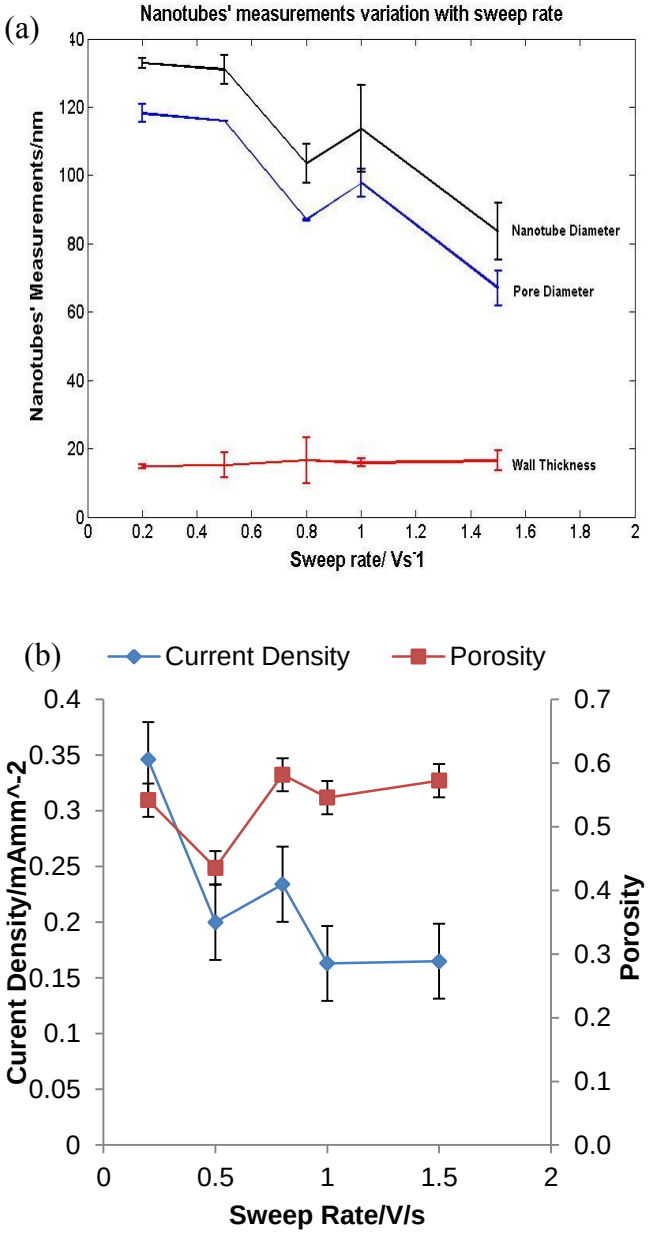

Figure 11: (a) Nanotube morphology and (b) Final Current value variation with pH

4V alloy and as such the vanadium to aluminium content is normally present in a higher quantity in the beta-phase than the alpha-phase [32][33][34]. The difference in the vanadium content in the alpha and beta phase accounted for more etching in the beta phase. The X-Ray analysis further showed the difference in Figure 14 (3.1 in alpha phase and 3.8 in beta phase).

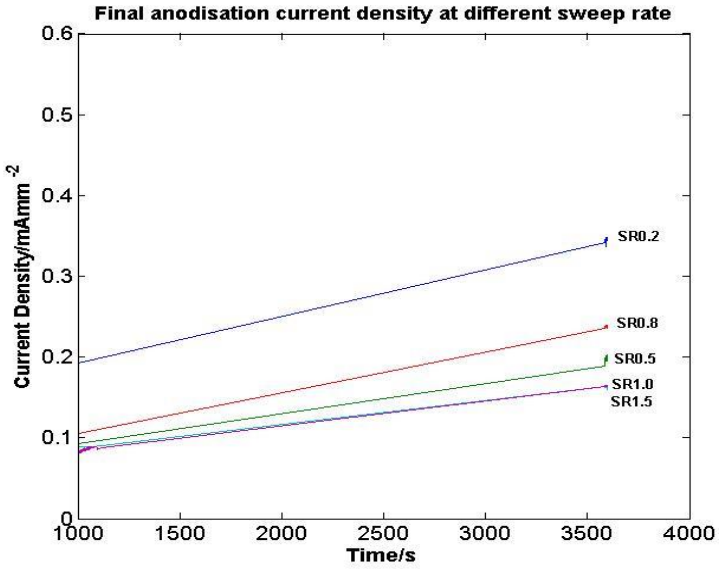

Figure 12: Variation of current density with time during the last 30 minutes of anodisation at different sweep rates

At 20 minutes (Figure 13 (d)), the porous structures in the beta phase, became nanograins while the alpha phase maintained the porous structures with thicker walls of the pores. The nanograins could be assumed to be the underlying alpha phase grains which developed into a thin layer of nanoporous layer five minutes later. Then these grains developed into nanoporous structures (~100nm) while the randomly arranged nanopores (<50nm) in the alpha phase became uniformly arranged nanotubes after 40 minutes. After one hour, the nanotubes had an average diameter of 100nm in the alpha phase as could be seen in Figure 13 (g). The beta phase contained similar sized nanopores alongside a smaller amount of smaller sized pores as well.

The above observations allowed a new perspective into the growth of nanotubes. Chen and colleagues did obtain a pattern in the growth of nanotubes on the surface of Ti-10Ta similar to what was obtained

in this study [11]. The anodisation started with randomly arranged porous structures and ended with uniformly arranged nanotubes. Meanwhile, Dikova and colleagues defined the mechanism behind the growth of nanotube on the surface of Ti-6Al-4V with the surface of their samples being coated up to 80% with nanotubes in 7 hours [26]. During the process, where they used just hydrofluoric acid (HF),

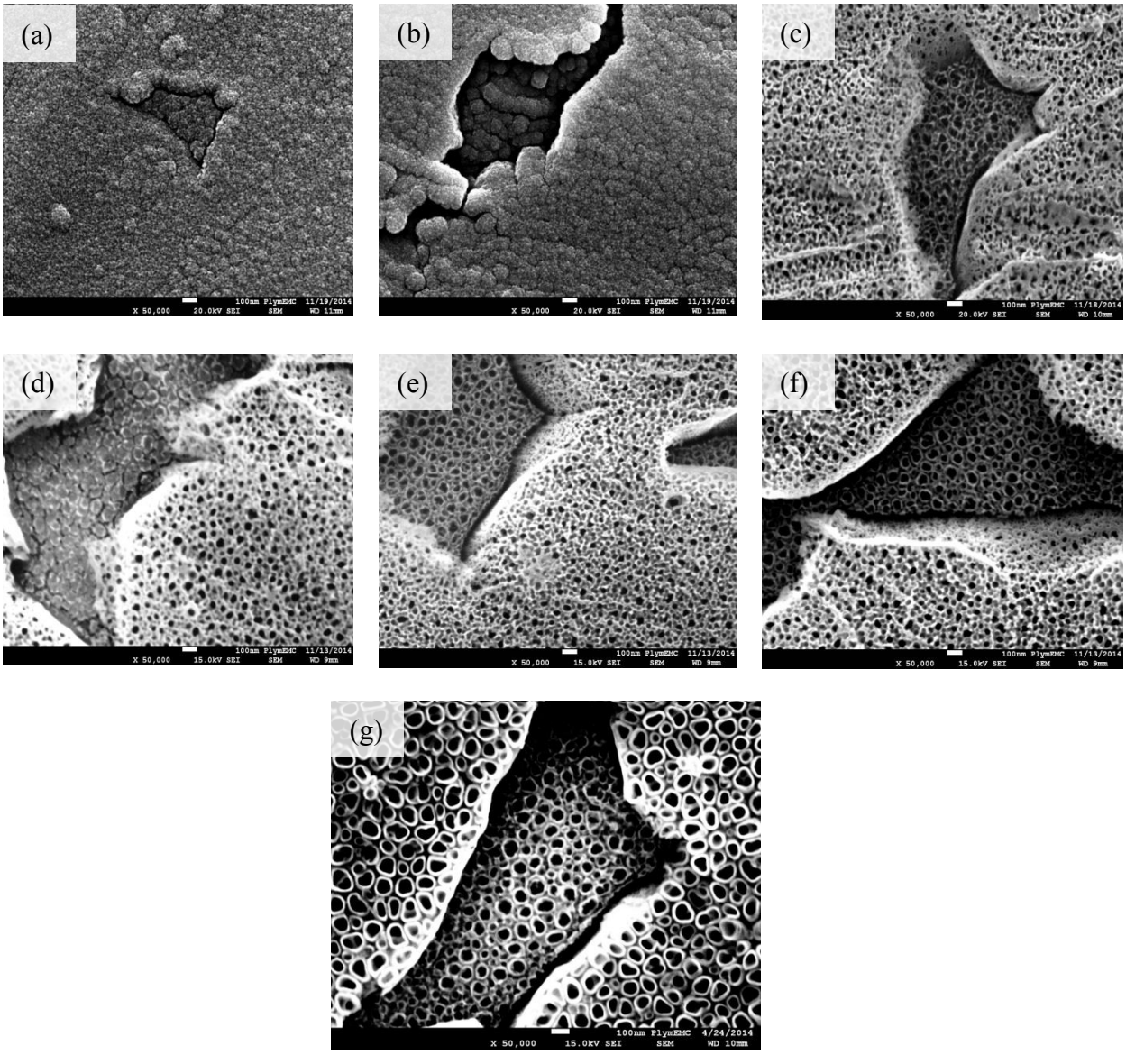

Figure 13: Coating grown at pH 4 and sweep rate 0.5 Vs^{-1} viewed at 50 000 magnification at (a) 5 minutes, (b) 10 minutes, (c) 15 minutes (d) 20 minutes, (e) 25 minutes, (f) 30 minutes and (g) 60 minutes of anodisation

the synthesis of the nanotubes started with the presence of nano-seeds. The latter looked different from the ones obtained in this study whereby nanograins with a rough surface structure were the first result of etching. It was only in the beta phase that the 'bowl-like' structures were grown on the titanium alloy used in this study (Figure 13 (d)). The buffering effect of the electrolyte being used in this study was responsible for this effect.

This analysis led to the mechanism behind nanotube assembly in the alpha- phase being as follows:

1) Formation of nanoparticles,
2) Development of 'doughnut-shaped' structures due to arrangement of the nanoparticles leading to the formation of pores slightly bigger than 200nm pore diameter.
3) Evolution of the nanoparticles and above mentioned structures into nanoporous structures, with varying diameters, all over the surface.
4) Growth of the nanoporous surface into nanotubes with solid wall and a distance in between each nanotube.

The nanoparticles formed, at the beginning, was due to the etching process in the presence of fluoride ions. Since fluoride ions have small diameter, they were able to force nano-cracks on the surface of the barrier-oxide layer. The latter led to the presence of the uniformly spread nanoparticles all over the surface of the sample. Since nanoparticles have the tendency to stick to each other, they arranged themselves in such a way that the doughnut-shaped structures were formed as shown in Figure 15. The presence of the pore inside the structure was due to the fluoride ions. Growth of similar structures all over the place led to the formation of the nanoporous layer. Since there was oxidation and

chemical dissolution at the same time, neighbouring, ‘doughnut-shaped’ structures was assumed to be stacked together so that the competition reactions and lateral forces resulted in the formation of the nanoporous surface. The pores in the nanoporous structures do have smaller pore diameters than the previous structures because oxidation was taking place at the same time as dissolution. This process continued for 30 min whereby the pores were arranged uniformly with solid walls differentiating the pores from each other. It was observed that there was a distance in between the walls of nanotubes. This followed the theory derived by the group of Schmuki whereby it was explained that as the nanotubes grew longer, the pore diameter decreased, accounting for larger base and smaller opening [29] .

3.6 Theory of initial etching sites

In this study, Ti-6Al-4V alloy was used and as such, during the anodisation process, the oxides of aluminium and vanadium was formed along with titanium dioxide.

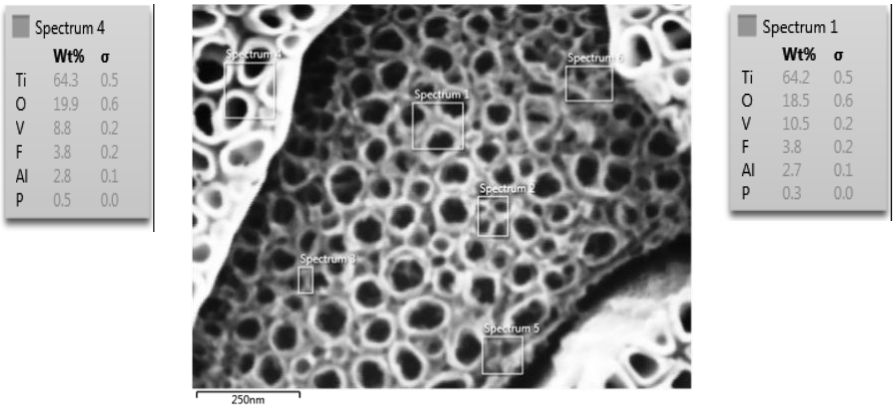

Figure 14: The EDS analysis results comparing the vanadium content in the alpha and beta phase.

Nonetheless, the discussion in this work was limited to the oxide of titanium only, due to the predominance of titanium over aluminium and vanadium on the coating (EDS analysis in Figure 14). Following the observations at different pH and sweep rate, a new theory was deduced which related the growth of nanotubes to the etching sites at very early stage. The effect of pH and sweep rate could

be illustrated using Figures 16 and 17 respectively.

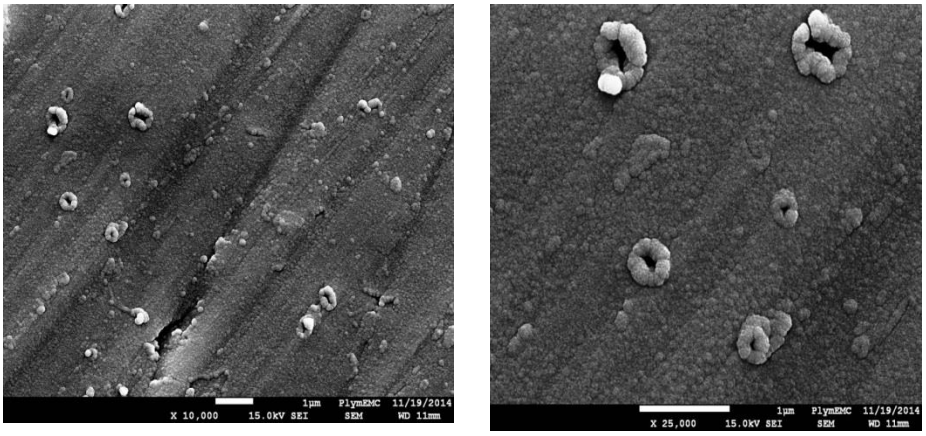

Figure 15: Presence of 'doughnut-shaped' structures at 5 minutes of anodisation at low magnification

Due to the large volumetric expansion in the oxidation process, the oxide layer is under large in-plane compressive stress. This could cause buckling or wrinkling according to Hutchinson and Suo (1992) [35]. The valley of the wrinkles is under additional surface energy and becomes preferred sites for etching. At lower pH, etching started earlier so that the barrier layer was thinner and less stressed. Fewer etching sites per unit area were expected so that smaller number of nanotubes per unit area compared to a higher pH. Figure 16 (a) illustrated that there are fewer nanotubes at lower pH. The wall is thinner while pores are larger due to the ongoing etching of the walls at higher concentration of hydrogen ions. Part (b) showed the growth of the nanotubes at a higher pH. Due to lower concentration of hydrogen ions and hence higher [OH^-], more oxide was deposited on the inner walls of the tubes. This caused the wall thickness to increase with time. Therefore nanotubes with thicker walls and smaller pores were obtained at a higher pH. This is in agreement with the images in Figure 6.

Figure 15 illustrated the effect of sweep rate on the growth. At a higher sweep rate, the reaction was quicker, resulting in a higher stress being generated accounting for more bulging and as such the presence of more etching sites with smaller size. It is expected that the in-plane stress due to the

oxidation expansion is proportional to the reaction rate.

This was imaged by Figure 17 whereby more nanotubes with much smaller pores were formed at higher sweep rate than at lower sweep rate. The final current density is determined by the etching rate which is determined by the impedance of the smaller pores. Therefore the final density decreases with increasing sweep rate due to higher impedance of the pores. Nevertheless the wall thickness is not significantly affected as shown in Figure 9(b).

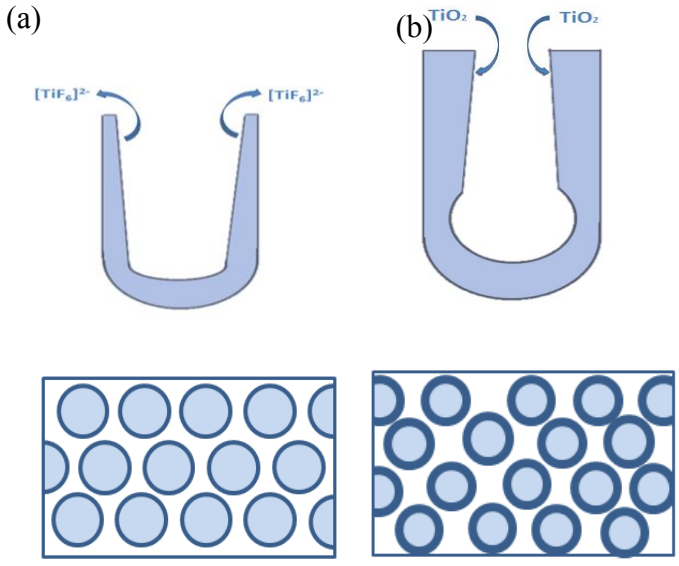

Figure 16: The nanotube morphology at (a) low pH and (b) high pH highlighting the dominating reaction taking place

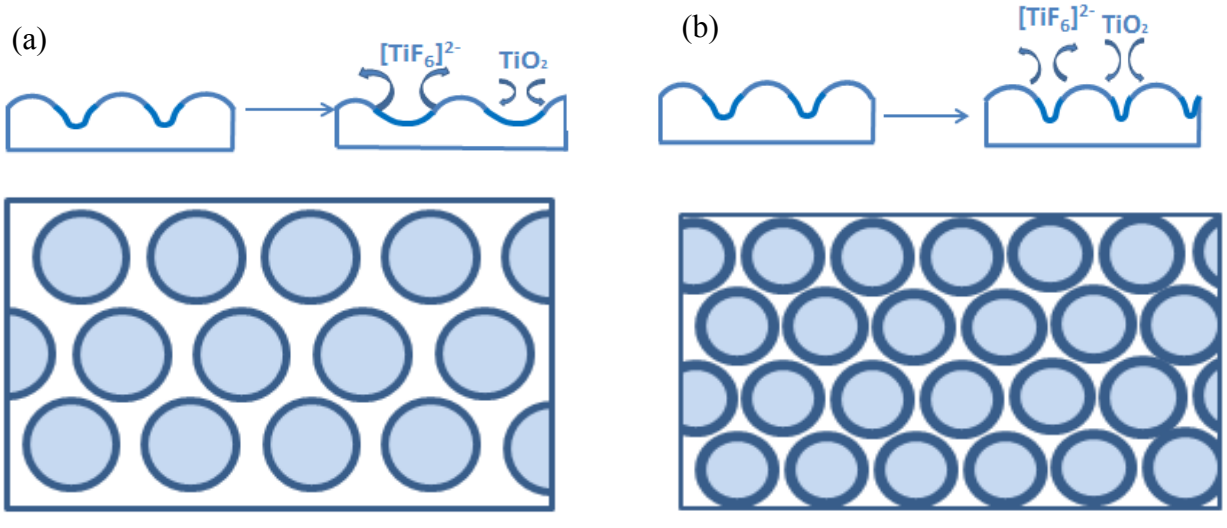

Figure 17: The nanotube morphology at (a) low sweep rate and (b) high sweep rate highlighting the main reaction taking place

In summary the rate of formation of barrier layer plays an important role. Higher the reaction rate leads to higher stress and hence higher density of nanotubes. In turn this will increases the impedance of the pores and reduces the growth rate.

4. Conclusions

This study proved that sweep rate did have a significant role to play in the self-assembly of titanium dioxide nanotubes as well as the pH of the electrolyte. The morphology was dependent on the rate at which the voltage was increased to the target value along with the concentration of hydrogen ions in the electrolytes. Furthermore, this research work provided a deeper insight to the different stages of the nano self-assembly which allowed a new theory related to the initial etching sites to be derived involving the formation of titanium dioxide nanotubes on the surface of Ti-6Al-4V, in the presence of phosphate ions. . This would be beneficial in carrying antibacterial agents in the nanotubes providing a good surface coverage.

Acknowledgements

The authors would like to acknowledge the funding through a joint PhD studentship for UD by the Faculty of Science and Environment and Peninsular Schools of Medicine and Dentistry is acknowledged. The assistance by the technical team in the School of Marine Science and Engineering and the Electron Microscopy Centre (EMC) of Plymouth University is gratefully acknowledged.

References

[1] N. H. Ahmad Barudin, S. Sreekantan, O. M. Thong, and L. K. Lay, "Studies of Cell Growth on TiO_2 Nanotubes," *Adv. Mater. Res.*, vol. 620, pp. 325–329, 2012.

[2] K. S. Brammer, C. J. Frandsen, and S. Jin, "TiO2 nanotubes for bone regeneration," *Trends Biotechnol*, vol. 30, no. 6, pp. 315–322, 2012.

[3] B. Feng, J. Weng, B. C. Yang, S. X. Qu, and X. D. Zhang, "Characterization of surface oxide films on titanium and adhesion of osteoblast," *Biomaterials*, vol. 24, pp. 4663–4670, 2003.

[4] L. M. Bjursten, L. Rasmusson, S. Oh, G. C. Smith, K. S. Brammer, and S. Jin, "Titanium dioxide nanotubes enhance bone bonding in vivo," *J Biomed Mater Res A*, vol. 92, no. 3, pp. 1218–1224, 2010.

[5] K. S. Brammer, S. Oh, C. J. Cobb, L. M. Bjursten, H. van der Heyde, and S. Jin, "Improved bone-forming functionality on diameter-controlled TiO(2) nanotube surface," *Acta Biomater*, vol. 5, no. 8, pp. 3215–3223, 2009.

[6] J. Park, S. Bauer, P. Schmuki, and K. von der Mark, "Narrow window in nanoscale dependent activation of endothelial cell growth and differentiation on TiO2 nanotube surfaces," *Nano Lett*, vol. 9, no. 9, pp. 3157–3164, 2009.

[7] N. Wang, H. Li, W. Lu, J. Li, J. Wang, Z. Zhang, and Y. Liu, "Effects of TiO2 nanotubes with different diameters on gene expression and osseointegration of implants in minipigs," *Biomaterials*, vol. 32, no. 29, pp. 6900–6911, 2011.

[8] M. Balakrishnan and R. Narayanan, "Synthesis of anodic titania nanotubes in Na2SO4/NaF electrolyte: A comparison between anodization time and specimens with biomaterial based approaches," *Thin Solid Films*, vol. 540, pp. 23–30, 2013.

[9] V. S. A. Challa, S. MAli, and R. D. K. Misra, "Reduced toxicity and superior cellular response of preosteoblasts to Ti-6Al-7Nb alloy and comparison with Ti-6Al-4V," *Soc. Biomater.*, vol. 101A, no. 7, pp. 2083–2089, 2013.

[10] J. Fojt, "Ti–6Al–4V alloy surface modification for medical applications," *Appl. Surf. Sci.*, vol. 262, pp. 163–167, 2012.

[11] X. Chen, K. Cai, J. Fang, M. Lai, J. Li, Y. Hou, Z. Luo, Y. Hu, and L. Tang, "Dual action antibacterial TiO2 nanotubes incorporated with silver nanoparticles and coated with a quaternary ammonium salt (QAS)," *Surf. Coatings Technol.*, vol. 216, pp. 158–165, 2013.

[12] L. Zhao, H. Wang, K. Huo, L. Cui, W. Zhang, H. Ni, Y. Zhang, Z. Wu, and P. K. Chu, "Antibacterial nano-structured titania coating incorporated with silver nanoparticles," *Biomaterials*, vol. 32, no. 24, pp. 5706–5716, 2011.

[13] W. Xin, C. Meng, W. Jie, T. Junchao, S. Yan, and D. Ning, "Nanotube Arrays on Anodization Variables and Buffer Medium," *J. Semicond.*, vol. 31, no. 6, p. 063003, 2010.

[14] J. M. Macak, H. Tsuchiya, and P. Schmuki, "High-aspect-ratio TiO2 nanotubes by anodization of titanium," *Angew Chem Int Ed Engl*, vol. 44, no. 14, pp. 2100–2102, 2005.

[15] D. Kowalski, D. Kim, and P. Schmuki, "TiO2 nanotubes, nanochannels and mesosponge: Self-organized formation and applications," *Nano Today*, vol. 8, no. 3, pp. 235–264, 2013.

[16] D. Kim, F. Schmidt-Stein, R. Hahn, and P. Schmuki, "Gravity assisted growth of self-organized anodic oxide nanotubes on titanium," *Electrochem. commun.*, vol. 10, pp. 1082–1086, 2008.

[17] B.-G. Lee, J.-W. Choi, S.-E. Lee, Y.-S. Jeong, H.-J. Oh, and C.-S. Chi, "Formation behavior of anodic TiO2 nanotubes in fluoride containing electrolytes," *Trans. Nonferrous Met. Soc. China*, vol. 19, no. 4, pp. 842–845, 2009.

[18] H. Tsuchiya, J. M. Macak, L. Taveira, E. Balaur, A. Ghicov, K. Sirotna, and P. Schmuki, "Self-organized TiO2 nanotubes prepared in ammonium fluoride containing acetic acid electrolytes," *Electrochem. commun.*, vol. 7, no. 6, pp. 576–580, 2005.

[19] Q. Cai, M. Paulose, O. Varghese, and C. A. Grimes, "The effect of electrolyte composition on the fabrication of self-organised titanium oxide nanotube arrays by anodic oxidation," *Mater. Res. Soc.*, vol. 20, no. 1, pp. 230–236, 2005.

[20] M. Paulose, O. K. Varghese, G. K. Mor, C. a. Grimes, and K. G. Ong, "Unprecedented ultra-high hydrogen gas sensitivity in undoped titania nanotubes," vol. 17, pp. 398–402, 2006.

[21] E. Matykina, J. M. Hernandez-López, a. Conde, C. Domingo, J. J. De Damborenea, and M. a. Arenas, "Morphologies of nanostructured TiO2 doped with F on Ti-6Al-4V alloy," *Electrochim. Acta*, vol. 56, pp. 2221–2229, 2011.

[22] Y. Q. Hao, S. J. Li, Y. L. Hao, Y. K. Zhao, and H. J. Ai, "Effect of nanotube diameters on bioactivity of a multifunctional titanium alloy," *Appl. Surf. Sci.*, vol. 268, pp. 44–51, 2013.

[23] C. P.-J. Peremarch, R. P. Tanoira, M. A. Arenas, E. Matykina, A. Conde, J. J. De Damborenea, E. G. Barrena, and J. Esteban, "Bacterial adherence to anodized titanium alloy," *J. Phys. Conf. Ser.*, vol. 252, p. 12011, 2010.

[24] S. Bauer, S. Kleber, and P. Schmuki, "TiO2 nanotubes: Tailoring the geometry in H3PO4/HF electrolytes," *Electrochem. commun.*, vol. 8, no. 8, pp. 1321–1325, 2006.

[25] L. V. Taveira, J. M. Macák, H. Tsuchiya, L. F. P. Dick, and P. Schmuki, "Initiation and Growth of Self-Organized TiO[sub 2] Nanotubes Anodically Formed in NH[sub 4]F / (NH[sub 4])[sub 2]SO[sub 4] Electrolytes," *J. Electrochem. Soc.*, vol. 152, p. B405, 2005.

[26] T. D. Dikova, M. G. Hahm, D. P. Hashim, N. T. Narayanan, R. Vajtai, and P. M. Ajayan, "Mechanism of TiO 2 Nanotubes Formation on the Surface of Pure Ti and Ti-6Al-4V Alloy," *Proc. AMPT2013*, vol. 939, p. CD–ROM, 2013.

[27] J. M. Macak, H. Tsuchiya, L. Taveira, A. Ghicov, and P. Schmuki, "Self-organized nanotubular oxide layers on Ti-6Al-7Nb and Ti-6Al-4V formed by anodization in NH4F solutions," *J Biomed Mater Res A*, vol. 75, no. 4, pp. 928–933, 2005.

[28] C. Zoski, *Handbook fo Electrochemistry*, First Edit. Netherland: Elsevier B.V., 2007.

[29] J. M. Macak, H. Tsuchiya, A. Ghicov, K. Yasuda, R. Hahn, S. Bauer, and P. Schmuki, "TiO2 nanotubes: Self-organized electrochemical formation, properties and applications," *Curr. Opin. Solid State Mater. Sci.*, vol. 11, no. 1–2, pp. 3–18, 2007.

[30] X. Chen, J. Chen, and J. Lin, "Self-assembled TiO2 nanotube arrays with U-shaped profile by controlling anodization temperature," *J. Nanomater.*, vol. 2010, pp. 1–4, 2010.

[31] A. Ghicov, H. Tsuchiya, J. M. Macak, and P. Schmuki, "Titanium oxide nanotubes prepared in phosphate electrolytes," *Electrochem. commun.*, vol. 7, no. 5, pp. 505–509, 2005.

[32] W. Z. K. K. and M. M. J. Sieniawski, "Titanium Alloys - Advances in Properties Control," pp. 70–80, 2013.

[33] L. Zeng and T. R. Bieler, "Effects of working, heat treatment, and aging on microstructural evolution and crystallographic texture of α, α', α'' and β phases in Ti-6Al-4V wire," *Mater. Sci. Eng. A*, vol. 392, pp. 403–414, 2005.

[34] B. Luo, H. Yang, S. Liu, W. Fu, P. Sun, M. Yuan, Y. Zhang, and Z. Liu, "Fabrication and characterization of self-organized mixed oxide nanotube arrays by electrochemical anodization of Ti-6Al-4V alloy," *Mater. Lett.*, vol. 62, pp. 4512–4515, 2008.

[35] J. W. Hutchinson and Z. Suo, "Mixed Mode Cracking in Layered Materials," *Advances in Applied Mechanics*, vol. 29. pp. 63–191, 1991.